



# CME-related Large Decreases in the Differential Phase Delay of Tianwen-1 DOR Signals

Qingbao He<sup>1</sup> , Zhichao Wang<sup>2,3</sup> , Qinghui Liu<sup>2</sup>, Kaijun Liu<sup>1</sup> , and Li Guo<sup>2</sup><sup>1</sup> Department of Earth and Space Sciences, Southern University of Science and Technology, Shenzhen 518055, People's Republic of China; [liukj@sustech.edu.cn](mailto:liukj@sustech.edu.cn)<sup>2</sup> Shanghai Astronomical Observatory, Chinese Academy of Sciences, Shanghai 200030, People's Republic of China<sup>3</sup> University of Chinese Academy of Sciences, Beijing 100049, People's Republic of China

Received 2022 August 23; revised 2022 October 27; accepted 2022 November 11; published 2022 November 30

## Abstract

Differential phase delay is calculated for the differential one-way range (DOR) signals transmitted by Tianwen-1, the first Chinese Mars spacecraft that entered into the Mars orbit on 2021 February 10. Large decreases in the differential phase delay are identified in the DOR signals received by ground stations on 2021 March 23 and June 18. The decreases indicate sizable increases of the total electron content (TEC) along the DOR signal path between Tianwen-1 and the ground stations. The TEC increases are estimated to be 85 and 175 TEC units on 2021 March 23 and June 18, respectively. Evidence shows that they are caused by the sheath regions ahead of the coronal mass ejections (CMEs) that traversed the signal path on both days. The results represent the first observations of CME-related structures by the DOR signals and demonstrate the potential of DOR signals in remote sensing the interplanetary plasma structures in the solar wind.

*Unified Astronomy Thesaurus concepts:* Solar wind (1534); Solar coronal mass ejections (310); Deep space probes (366); Radio astronomy (1338); Remote sensing (2191)

## 1. Introduction

The first Chinese Mars spacecraft, Tianwen-1, was launched on 2020 July 23 and entered into the Mars orbit on 2021 February 10. On 2021 May 15, the capsule containing a lander and a rover separated from the orbiter, and made a soft landing on the Mars surface (Zou et al. 2021; Zhang et al. 2022). During the mission, a high gain antenna on board the orbiter kept transmitting differential one-way range (DOR) signals in the X band (~8.4 GHz). In the frequency domain, the DOR signals contain five spectral lines spanning a range of 38.4 MHz. They were received by the Chinese very long baseline interferometry (VLBI) network to improve the accuracy of Tianwen-1's orbit determination (Liu et al. 2022; Yang et al. 2022). The Chinese VLBI network includes four ground radio telescopes, which are Tianma (TM; 65 m), Beijing (BJ; 50 m), Kunming (KM; 40 m), and Urumqi (UR; 25 m) (Liu et al. 2014; He et al. 2017).

The interplanetary solar wind plasma has influence on the DOR signals when they propagate between the spacecraft and Earth. Just like how the Global Positioning System (GPS) signals have been widely used to derive the total electron content (TEC) variations in the Earth's ionosphere (Ho et al. 1996), the differential phase delay of the Tianwen-1 DOR signals might provide information on the interplanetary plasma structures along the signal path between the spacecraft and the VLBI ground stations. Given that the average distance between Mars and Earth is about 1.5 au, a moderate density change related to a sufficiently large-scale interplanetary plasma structure can produce a considerable TEC change that can show up in the DOR signals. In the present study, we calculate the differential phase delay of the Tianwen-1 DOR signals and derive the corresponding TEC variations along the signal path. The contribution of Earth's ionosphere to the TEC variations is

removed using Global Navigation Satellite System (GNSS) data (Zhou et al. 2021). The results show that the interplanetary plasma TEC increases dramatically on certain days. The big increases (and increase rates) are much higher than that Earth's ionosphere typically causes. Since the minimum distance of the signal path to the Sun was over 0.59 au on these days, the TEC changes should be related to the interplanetary solar wind plasma structures instead of variations in the solar corona. Further evidence suggests that they are caused by the sheath regions ahead of the coronal mass ejections (CMEs) passing through the signal path.

A number of experiments have been performed using ranging/Doppler data to probe the plasma near the Sun, including Pioneer series, Mariner series, Helios 1 and 2, and Viking, and the changes in signals' group and phase velocities were measured to determine the TEC of the solar corona (see Table II in Bird 1982). More recent interplanetary missions, including Mars Express, Venus Express, Rosetta, Ulysses, and Voyager, also used dual-frequency ranging data to probe the corona region (Anderson et al. 1987; Bird et al. 1994; Patzold et al. 2012; Efimov et al. 2013, 2017). Those experiments were mostly focused on superior solar conjunctions, and the dual frequencies used are spaced in very large frequency ranges, for example, one in the X band and the other in the S band. The present study demonstrates the first remote sensing of interplanetary solar wind density changes using narrowband DOR signals. The rest of the Letter is organized as follows. Section 2 introduces the methodology of data processing. Section 3 presents the results of two cases with sharp changes in the differential phase delay. Section 4 provides evidence to show that the changes are caused by the sheath regions ahead of the CMEs passing through the signal path. Section 5 concludes the Letter. Note that time is in coordinated universal time (UTC) throughout the Letter.

## 2. Methodology

The Tianwen-1 Mars orbiter transmits DOR signals in the X band, which are phase modulated over a carrier wave. The

signals are recorded by the Chinese VLBI stations at five frequencies: 8411.8 MHz, 8427.2 MHz, 8431.0 MHz (carrier), 8434.8 MHz, and 8450.2 MHz (Liu et al. 2022). In the present study, the differential phase delay between the DOR signals at 8411.8 MHz (the lowest frequency) and 8450.2 MHz (the highest frequency) is calculated following the method described in He et al. (2021). Note that He et al. (2021) analyzed the DOR signals of the Chinese lunar spacecraft, Chang'E-3, and were concerned about the influence of signal reflection from the spacecraft and lunar surfaces. For the DOR signals of Tianwen-1, however, the influence of signal reflection can be neglected as the DOR signals are transmitted by a high gain antenna on board the Mars orbiter. Thus, the total phase of the DOR signal at a specific frequency  $f_i$  can be represented as

$$\phi_i = 2\pi(f_i + f_{d,i})t + \phi_{\text{ins},i} + \phi_{\text{atm},i} + \phi_{\text{ion},i} + \phi_{\text{pla},i} + \theta_i, \quad (1)$$

where  $\phi_i$  is the total phase;  $f_i$  is the signal frequency transmitted from the spacecraft;  $f_{d,i}$  is the Doppler-shift frequency;  $t$  is the signal travel time;  $\phi_{\text{ins},i}$ ,  $\phi_{\text{atm},i}$ ,  $\phi_{\text{ion},i}$ , and  $\phi_{\text{pla},i}$  are the phases caused by the ground instrument, the Earth's atmosphere and ionosphere, and the interplanetary plasma, respectively; and  $\theta_i$  is the initial phase. Dividing Equation (1) by  $f_i$  gives the phase delay, and subtracting the phase delays at two frequencies yields the differential phase delay,

$$\Delta\tau_{12} = \Delta\tau_{\text{ins},12} + \Delta\tau_{\text{ion},12} + \Delta\tau_{\text{pla},12} + \Delta\tau_{\theta,12}, \quad (2)$$

where  $\Delta\tau_{12}$  represents the differential phase delay and  $\Delta\tau_{\text{ins},12}$ ,  $\Delta\tau_{\text{ion},12}$ ,  $\Delta\tau_{\text{pla},12}$ , and  $\Delta\tau_{\theta,12}$  are the differential delays caused by the ground instrument, the Earth's ionosphere, the interplanetary plasma, and the initial phases, respectively. The phase delay caused by the Earth's atmosphere does not vary with signal frequency, so its influence disappears in the differential phase delay. In addition, since the DOR signals are received by different channels at ground stations,  $\Delta\tau_{\text{ins},12}$  is not zero but can be considered as a constant within a few hours (Zheng et al. 2014).  $\Delta\tau_{\text{ion},12}$  may experience small variations that can be mostly removed using GNSS data. Finally,  $\Delta\tau_{\theta,12}$  is a constant. Therefore, large variations in the differential phase delay must be caused by the interplanetary solar wind structures. It should be clarified that the absolute value of the interplanetary plasma influence cannot be obtained from Equation (2), but only its relative changes are relevant. So we shift the differential phase delay of each scan calculated from Equation (2) to be around zero by subtracting its mean value from it.

During the Tianwen-1 mission, the Chinese VLBI stations alternately observe the spacecraft and reference quasars for calibration. This leads to temporal gaps in the differential phase delay. In order to better demonstrate the overall changing trend of the differential phase delay, we use linear fitting and extrapolated values to connect the consecutive scans of the differential phase delay. Eventually, the differential phase delay obtained (after the influence of the Earth's ionosphere is removed using GNSS data) can be related to TEC changes in the interplanetary plasma in the downlink path through

(Bird et al. 1996)

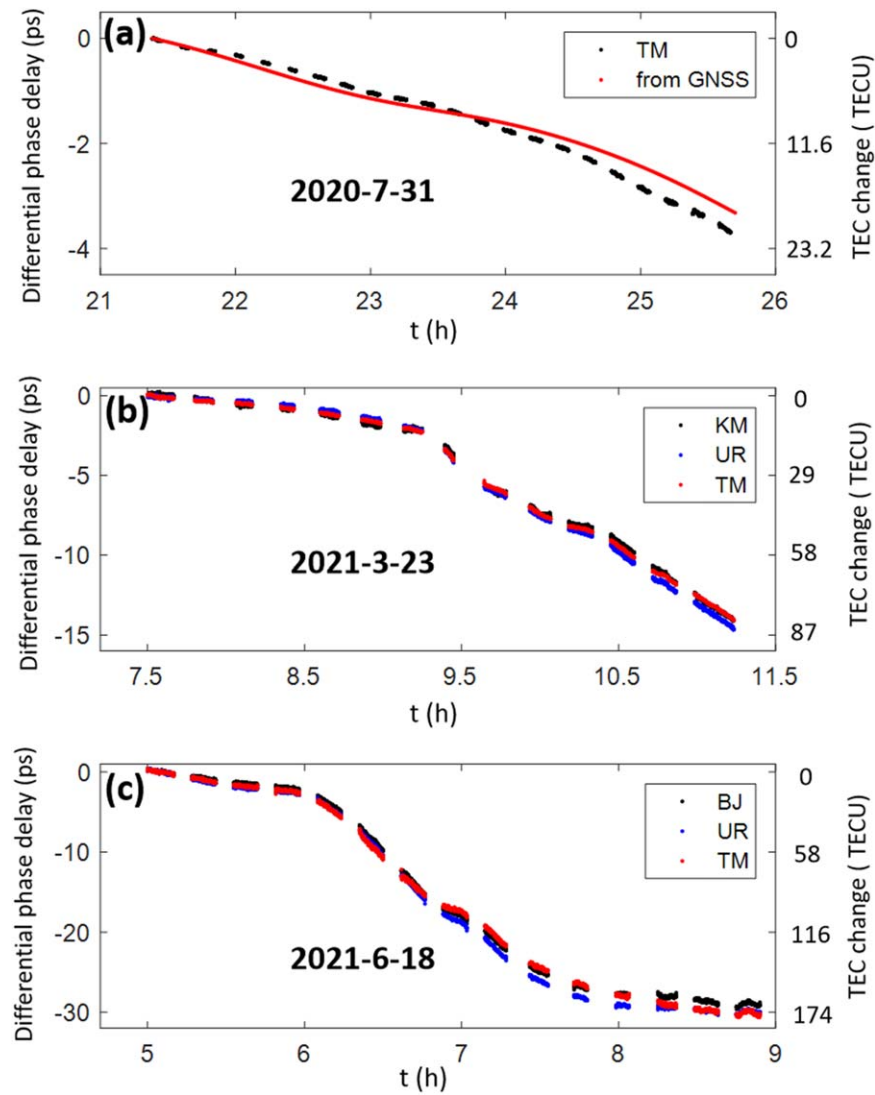
$$D = -\frac{c}{40.31} \cdot \frac{f_1^2 f_2^2}{f_2^2 - f_1^2} \cdot \Delta\tau_{12}, \quad (3)$$

where  $D$  is the TEC change and  $c$  is the light speed. Equation (3) shows that the TEC change is inversely proportional to the differential phase delay.

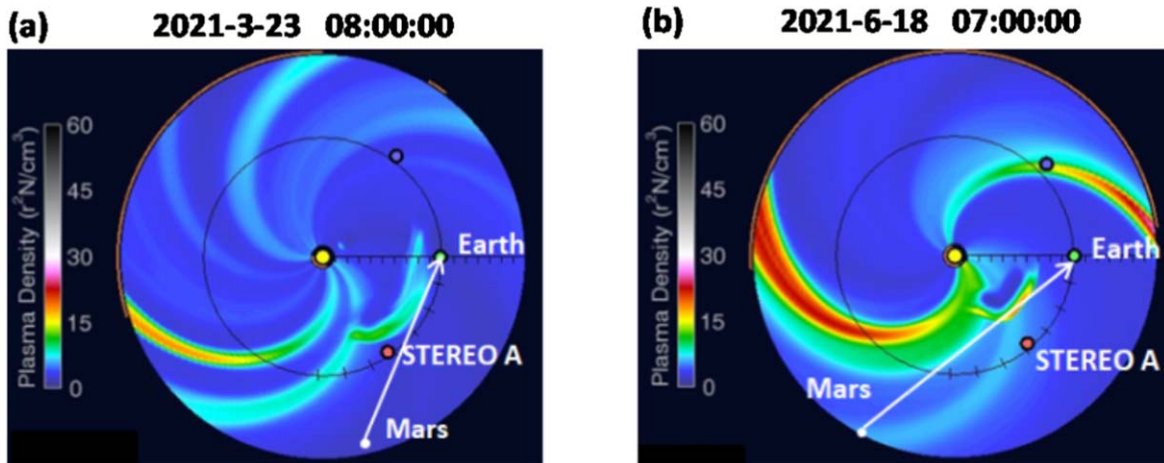
### 3. Data Processing Results

Figure 1 displays the differential phase delay calculated following the procedure described in Section 2 for three intervals on 2020 July 31, 2021 March 23, and 2021 June 18 as labeled. The time after 24 hr in Figure 1(a) represents the early morning of 2020 August 1. The corresponding TEC change is shown by the vertical axis on the right in each panel (in units of TECU, 1 TECU =  $10^{16}$  electrons  $\text{m}^{-2}$ ) following Equation (3). Note that the differential phase delay shown in Figure 1(a) for 2020 July 31 still contains the contribution of the Earth's ionosphere. Tianwen-1 was only about 2.5 million km (0.017 au) away from the Earth on that day, so variation of the differential phase delay is dominated by the contribution of the Earth's ionosphere. During the period shown, the differential phase delay declines about 3.7 ps, which suggests a TEC increase of about 21 TECU in the Earth's ionosphere. The ionosphere-related differential phase delay calculated from the GNSS data is plotted as the red curve in Figure 1(a), which indeed nicely follows the differential phase delay given by the Tianwen-1 DOR signals (the black curve). Note that UTC 21:00 corresponds to 05:00 Beijing Time, so the TEC increase reflects the regular local ionosphere variation at sunrise. The good agreement between the red and black curves also shows that our removal of the contribution of the Earth's ionosphere using GNSS data is reliable.

Tianwen-1 reached Mars on 2021 February 10 and started orbiting the planet since then. The differential phase delay calculated from its DOR signals demonstrates moderate variations most of the time but decreases dramatically on some days. Figures 1(b) and (c) present two such events that occurred on 2021 March 23 and June 18, respectively. Note that the observation on those two days only lasted for around 4 hr, so there is no data available after the intervals shown. Different from Figure 1(a), the influence of the Earth's ionosphere has been removed using GNSS data. The curves of different colors represent the results from the DOR signals received by the different ground stations as indicated by the legends. As expected, the curves agree with each other very well. More importantly, the differential phase delay demonstrates large drops over the intervals of  $\sim 4$  hr. Comparing with Figure 1(a), it is clear that not only the magnitudes of the drops but also their change rates are much larger than that of the typical differential phase delay variations related to the Earth's ionosphere. The large decreases of the differential phase delay correspond to TEC increases of about 85 and 175 TECU on 2021 March 23 and June 18, respectively. The orbit information of Tianwen-1 shows that the minimum distance of the DOR signal path to the Mars was more than 5000 km during the two intervals. So the signal path was far above the Martian ionosphere. On the other hand, the minimum distance of the signal path to the Sun was about 0.93 au and 0.59 au (200 and 129 solar radii) on the two days, respectively. This effectively rules out the possibility that the large differential



**Figure 1.** Differential phase delays and their corresponding TEC changes (right axes) during selected time intervals on 2020 July 31 (a), 2021 March 23 (b), and 2021 June 18 (c), respectively. The differential phase delay in (a) contains the influence of the Earth’s ionosphere, while the ionosphere contribution has been removed in the differential phase delays shown in (b) and (c). The red curve in (a) is the Earth’s ionosphere TEC change calculated from GNSS data.



**Figure 2.** Solar wind structures on 2021 March 23 (a) and 2021 June 18 (b) predicted by the WSA–Enlil model. The Earth and Mars positions and the corresponding DOR signal path are also marked.

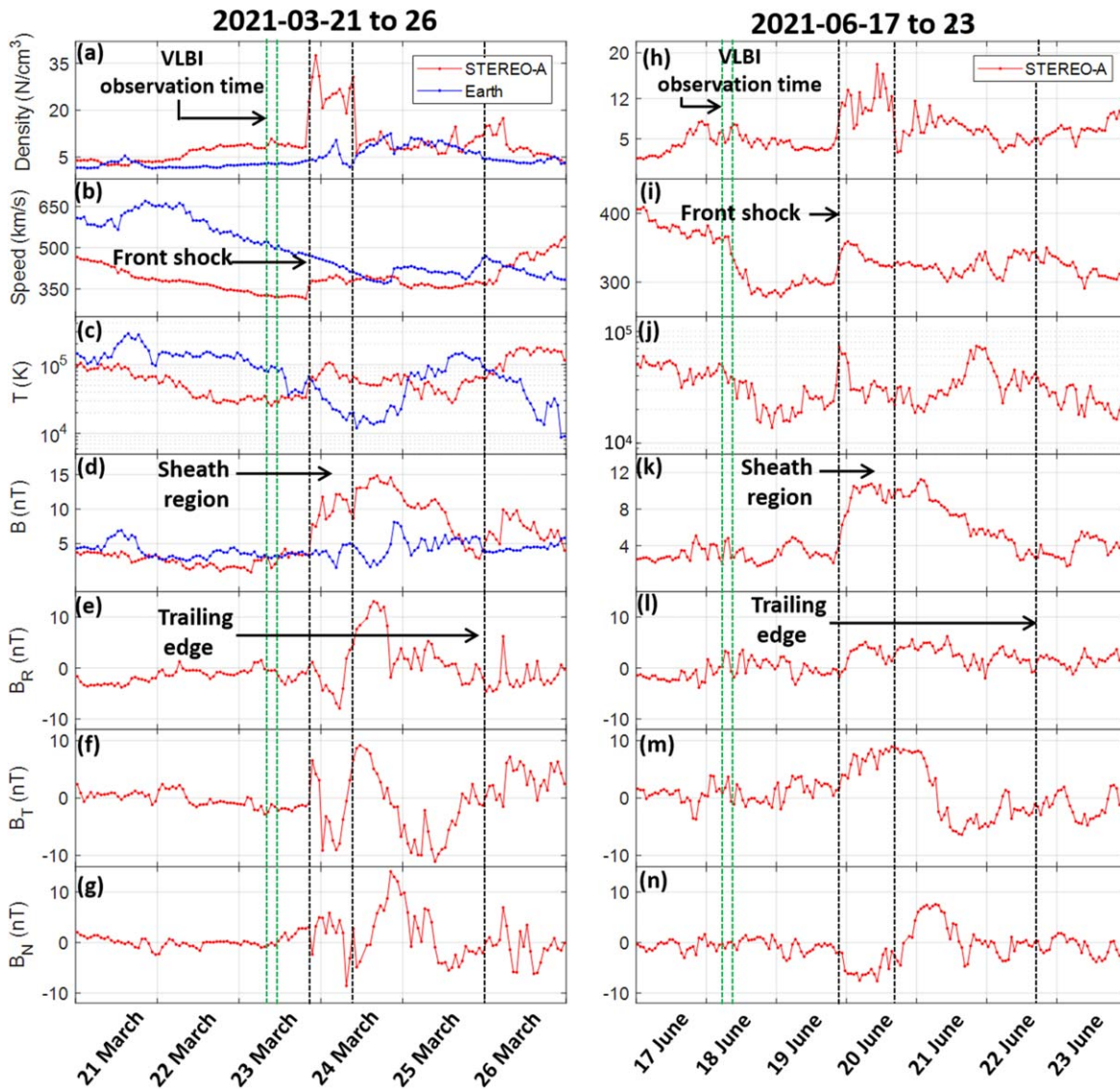


**Figure 3.** Solar wind parameters from 2021 March 21 to 26 (a)–(g) and from 2021 June 17 to 23 (h)–(n). From top to bottom in each column, the red curves display the solar wind density, speed, temperature, total magnetic field, and the three magnetic field components in the radial–tangential–normal coordinates ( $B_R$ ,  $B_T$ , and  $B_N$ ) observed by STEREO A, respectively. The blue curves in Figure 3(a)–(d) present the solar wind density, speed, temperature, and the total magnetic field near Earth. The two pairs of green vertical dashed lines delineate the VLBI observation time ranges on 2021 March 23 and June 18, respectively. The three black vertical dashed lines in each column mark the front shocks, sheath regions, and the trailing edges of the CMEs observed by STEREO A.

phase delay decreases observed are caused by variations in the solar corona. They should be related to some interplanetary plasma structures traversing the signal path, which can be CMEs.

#### 4. Discussion

Figure 2 displays the solar wind structures at 08:00 on 2021 March 23 and at 07:00 on 2021 June 18, which are obtained from the Wang–Sheeley–Arge (WSA)–Enlil online archive through the National Centers for Environmental Information of National Oceanic and Atmospheric Administration (NOAA). WSA–Enlil is a large-scale, physics-based prediction model of the heliosphere used by the NOAA Space Weather Forecast Office (Space Weather Prediction Center 2022). In Figure 2, the Earth and Mars positions are also marked, and the white arrows indicate the corresponding DOR signal path on the two days. It can be seen that CMEs are predicted on both days and they are passing through the Tianwen-1 DOR signal path.

As further evidence, Figure 3 shows the solar wind parameters measured by STEREO A (Bemporad 2011) from 2021 March 21 to 26 (panels (a)–(g)) and from 2021 June 17 to 23 (panels (h)–(n)) as red curves. Note that the positions of STEREO A on 2021 March 23 and June 18 have been illustrated in Figure 2. From top to bottom, the different panels in the two columns of Figure 3 present the solar wind density, speed, temperature, total magnetic field, and the three magnetic field components in the radial–tangential–normal coordinates ( $B_R$ ,  $B_T$ , and  $B_N$ ), respectively. For comparison, the solar wind density, speed, temperature, and the total magnetic field near the Earth from 2021 March 21 to 26 are shown as the blue curves in Figures 3(a)–(d). All the measurements shown in Figure 3 are obtained from the OMNI website (Papitashvili & King 2020).

Consistent with the solar wind structure predicted by the WSA–Enlil model shown in Figure 2(a), the solar wind density measured by STEREO A increases sharply on 2021 March 23. There are also corresponding variations in the other solar wind

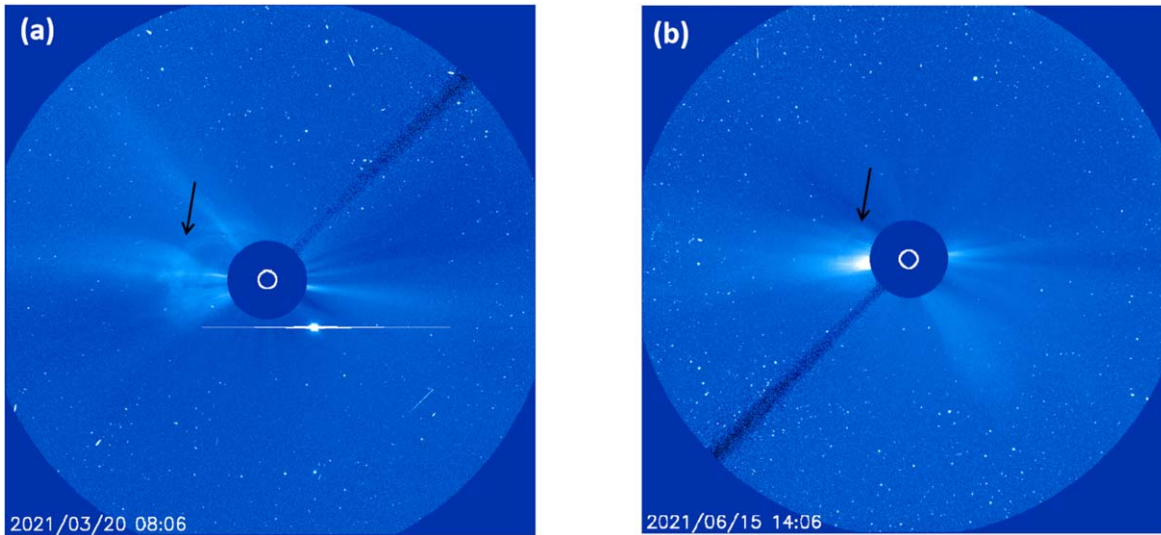


**Figure 4.** White-light solar corona images observed by SOHO/LASCO-C3 on 2021 March 20 (a) and 2021 June 15 (b). The black arrows point to the CMEs.

parameters shown, indicating a CME structure in the solar wind (Manchester et al. 2014; Nieves-Chinchilla et al. 2022). The solar wind parameters near the Earth also demonstrate large variations on 2021 March 24, suggesting (the edge of) a CME passing through. Similarly, STEREO A observed a CME structure starting on 2021 June 19, as shown in the right column of Figure 3. The front shocks, sheath regions, and the trailing edges of the CMEs are roughly indicated with the three black vertical dashed lines in each column of Figure 3. In addition, the two pairs of green vertical dashed lines in the left and right columns of Figure 3 delineate the VLBI observation time ranges on 2021 March 23 (Figure 1(b)) and June 18 (Figure 1(c)), respectively.

Overall, the observed differential phase delays (Figures 1(b) and (c)) start with a mild decrease and then experience a sharp drop, which should correspond to the sharp density increase near the front shocks in Figures 3(a) and (h). The observation time intervals of the differential phase delay decreases are about 4 hr, much shorter than the CME structures observed by STEREO A. Therefore, they should be more exactly related to the sheath regions as marked in Figure 3.

Furthermore, we check the Solar and Heliospheric Observatory (SOHO) spacecraft to find extra support for the CMEs predicted by the WSA–Enlil model. The Large Angle and Spectrometric Coronagraph (LASCO) on board SOHO is composed of three white-light coronagraph telescopes that image the solar corona from 1.5 to 32 solar radii (Patzold et al. 2012). Based on the WSA–Enlil model prediction, the CMEs shown in Figures 2(a) and (b) were ejected from the Sun on 2021 March 20 and June 15, respectively. Accordingly, the solar corona images observed by the C3 telescope of LASCO on 2021 March 20 and June 15 are shown in Figures 4(a) and (b), respectively, with the CMEs pointed by the black arrows.

All the evidence discussed above suggests that the large differential phase delay decreases shown in Figures 1(b) and (c) are caused by the sheath regions ahead of the CMEs traversing the Tianwen-1 DOR signal paths on the two days. The durations of the decreases shown are about 4 hr. The corresponding TEC increases are around 85 TECU (Figure 1(b)) and 175 TECU (Figure 1(c)) on 2021 March 23 and June 18, respectively. The scales of the plasma structures that have passed through the Tianwen-1 signal paths and caused the

observed differential phase delay decreases can then be estimated as below. The radial velocities of the sheath regions for the events of 2021 March 23 and June 18 are assumed as  $385 \text{ km s}^{-1}$  (see Figure 3(b)) and  $360 \text{ km s}^{-1}$  (see Figure 3(i)), respectively. In addition, the plasma density enhancements are assumed to be  $19 \text{ cm}^{-3}$  (see Figure 3(a)) and  $22 \text{ cm}^{-3}$ , respectively. Note that the plasma density enhancement in the sheath region observed by STEREO A at  $\sim 1 \text{ au}$  on 2021 June 19 is about  $8 \text{ cm}^{-3}$  (see Figure 3(h)), but the CME structure is about 0.6 au away from the Sun on 2021 June 18 and the plasma density is expected to vary approximately as  $1/r^2$  (where  $r$  is the radial distance from the Sun). With the parameters listed above, the scales of the sheath regions traversing the Tianwen-1 DOR signal paths on 2021 March 23 and June 18 are estimated to be  $0.037 \text{ au} \times 0.30 \text{ au}$  and  $0.035 \text{ au} \times 0.53 \text{ au}$ , respectively. Here the first number of the scales represents the size in the radial direction, while the other number indicates the length along the signal path.




## 5. Conclusion

Differential phase delay is calculated for the Tianwen-1 DOR signals with a bandwidth of 38.4 MHz. The results show that it experiences moderate variations on most days but large decreases on 2021 March 23 and June 18. Since the influence of the Earth’s ionosphere has been mostly removed and because the DOR signal path was high above the Martian ionosphere and far away from the solar corona, the large decreases could only be caused by the interplanetary solar wind structures traversing the DOR signal path on the two days. The solar wind structures predicted by the WSA–Enlil model for these two days as well as the corresponding in situ solar wind measurements and the corona images observed by SOHO support the scenario that the sheath regions ahead of two CMEs have passed through the signal path and caused the large differential phase delay decreases. The present study represents the first observations of CME-related structures by DOR signals and suggests that DOR signals can be valuable for remote sensing the interplanetary solar wind structures.

We are grateful to people in the Shanghai VLBI center who have participated in the Tianwen-1 mission for providing the

DOR signal data. We would also like to thank Dr. Fei Yao, Dr. Ying Xiong, Yan Wang, Xianming Zheng, Yuqi Liu, and Jingyi Zhou for helpful discussions. This work was supported by Strategic Priority Research Program of Chinese Academy of Sciences (grant No. XDB 41000000), NSFC grants 41974168 and 42174203, and Shenzhen Science and Technology Program (grant Nos. JCYJ20190809153407516 and JCY20210324104810027). It was also supported by the Center for Computational Science and Engineering of Southern University of Science and Technology and China Postdoctoral Science Foundation (2021M691442).

### ORCID iDs

Qingbao He  <https://orcid.org/0000-0003-2605-7083>  
 Zhichao Wang  <https://orcid.org/0000-0001-9234-3921>  
 Kaijun Liu  <https://orcid.org/0000-0001-5882-1328>

### References

- Anderson, J. D., Krisher, T. P., Borutzki, S. E., et al. 1987, *ApJ*, **323**, 141  
 Bemporad, A. 2011, *JASTP*, **73**, 1117  
 Bird, M. K. 1982, *SSRv*, **33**, 99  
 Bird, M. K., Paetzold, M., Edenhofer, P., et al. 1996, *A&A*, **316**, 441  
 Bird, M. K., Volland, H., Paetzold, M., et al. 1994, *ApJ*, **426**, 373  
 Efimov, A. I., Lukanina, L. A., Rudash, V. K., et al. 2013, *CosRe*, **51**, 13  
 Efimov, A. I., Lukanina, L. A., Samoznaev, L. N., et al. 2017, *AdSpR*, **59**, 1652  
 Ho, C. M., Mannucci, A. J., Lindqwister, U. J., Pi, X., & Tsurutani, B. T. 1996, *GeoRL*, **23**, 3219  
 He, Q., Liu, K., Ye, S., Liu, Q., & Deng, T. 2021, *AdSpR*, **68**, 4088  
 He, Q., Liu, Q., & Zheng, X. 2017, *RaSc*, **52**, 235  
 Liu, Q., Huang, Y., Shu, F., et al. 2022, *SSPMA*, **52**, 1  
 Liu, Q., Zheng, X., Huang, Y., et al. 2014, *RaSc*, **49**, 1080  
 Manchester, W. B., van der Holst, B., & Lavraud, B. 2014, *PPCF*, **56**, 1  
 Nieves-Chinchilla, T., Alzate, N., Cremades, H., et al. 2022, *ApJ*, **930**, 1  
 Patzold, M., Hahn, M., Tellmann, S., et al. 2012, *SoPh*, **279**, 127  
 Papitashvili, N. E., & King, J. H. 2020, OMNI Combined Heliospheric Observations (COHO), Merged Magnetic Field, Plasma and Ephemeris, Definitive Hourly Data, NASA Space Physics Data Facility, Accessed: 20 March 2022, doi:10.48322/6ffx-3441  
 Space Weather Prediction Center 2022, Wang-Sheeley-Arge (WSA)-Enlil Solar Wind Prediction, NOAA National Centers for Environmental Information, doi:10.7289/V5445JGH  
 Yang, P., Huang, Y., Li, P., et al. 2022, *AdSpR*, **69**, 1060  
 Zheng, X., Liu, Q., Wu, Y., et al. 2014, *J. Astronaut.*, **35**, 1030  
 Zhou, W., Song, S., Li, P., et al. 2021, *Journal of Deep Space Exploration*, **7**, 362  
 Zou, Y., Zhu, Y., Bai, Y., et al. 2021, *AdSpR*, **67**, 812  
 Zhang, A. B., Kong, L. G., Li, W. Y., et al. 2022, *E&PP*, **6**, 1